Applied Catalysis B: Environmental 84 (2008) 758–765

Contents lists available at ScienceDirect

Applied Catalysis B: Environmental

journal homepage: www.elsevier.com/locate/apcatb

# Studies on combustion catalytic activity of some pure and doped lanthanum cobaltites

Magdalena Bosomoiu [a], Grigore Bozga [a,*], Daniela Berger [b], Cristian Matei [b]

[a] Department of Chemical Engineering, University "Politehnica" of Bucharest, Polizu street no. 1, Bucharest 011061, Romania
[b] Department of Inorganic Chemistry, University "Politehnica" of Bucharest, Polizu street no. 1, Bucharest 011061, Romania

ARTICLE INFO

*Article history:*
Received 21 April 2008
Received in revised form 7 June 2008
Accepted 11 June 2008
Available online 18 June 2008

*Keywords:*
Catalysis
Combustion
Kinetics
Packed bed
Parameter identification
Perovskites

ABSTRACT

The aim of this work is to compare the catalytic activity of some pure and doped lanthanum cobaltites, prepared by solution combustion technique, with a $Pt/Al_2O_3$ commercial catalyst. As test reaction we used the combustion of lean methane mixtures. The experimental data evidenced a significantly better catalytic activity of a cerium-doped lanthanum cobaltite, prepared by using α-alanine as fuel. The combustion data, for the lean methane mixtures we tested, are well fitted by a first-order kinetic expression. The calculated activation energy values are in good agreement with the published data.



## 1. Introduction

In the last decades, catalytic combustion has received great attention, being one of the methods successfully applied in volatile organic compounds (VOC) removal from gaseous effluents and in the green energy production. Generally, the commercial catalysts used in this aim are noble metals dispersed on porous supports (e.g., platinum or palladium on alumina, etc.). Although noble metal catalysts are very active in the catalytic combustion, they are rather expensive and susceptible to deactivation by poisoning, particularly in the presence of compounds containing chlorine, sulphur, phosphorus, or in presence of water, one of the combustion products. Therefore, there is a high interest to replace noble metal catalysts by cheaper catalysts resistant to deactivation phenomena. Among other alternatives, the perovskite-type oxides are the most promising catalysts for VOC's combustion. In the perovskite general formula, $ABO_3$, the atoms A (usually a rare earth metal) and B (a transition metal) can be replaced in various percents with different cations A′ and B′, respectively, leading to a large class of compounds having the structure $A_{1-x}A'_xB_{1-y}B'_yO_3$ with different catalytic properties. The preparation procedure of these catalysts is of fundamental importance to determine phase stability of the active component and the resistance to the loss of active sites by sintering [1]. A survey of experimental data available in the literature shows that lanthanum-based perovskites exhibit good thermal stability and high activity [2–5]. Some authors reported half conversion temperature ($T_{50}$) values of around 500 °C for methane combustion over $La_{1-x}Ce_xCoO_3$ ($x = 0$–$0.5$), synthesized by citrate method [4]. $La_{0.8}Sr_{0.2}CoO_3$ prepared by coprecipitation method was found to be highly effective for cyclohexane, toluene and propyl alcohol combustion [6]. Several authors proposed the use of perovskite oxides as a support for noble metals [7–9]; Civera et al. [8] reported a relatively low $T_{50}$ value (432 °C) for methane combustion over 2 wt.% Pd deposited on $LaMnO_3{\cdot}2ZrO_2$. Chiarello et al. [10] prepared and characterized a 0.5 wt.% Pd supported on nano-sized $LaCoO_3$ perovskite. The easiness of toluene combustion over 0.5 wt.% Pd supported on perovskites oxides was found to decrease as follows: $Pd/LaFeO_3 > Pd/LaMnO_{3+\delta} > Pd/LaCoO_3 > Pd/LaNiO_3$ [11]. High activities were reported for ethanol combustion over strontium and cerium-doped $LaCoO_3$ catalyst when these are supported on $La$–$Al_2O_3$ [12]. Royer et al. [13] observed that cobalt-based perovskite was more active in methane combustion than the manganese-based perovskite, even if its specific surface area was lower. The strontium- and cerium-substituted samples were found to be only slightly more active than the pure $LaMnO_3$ sample, especially at low temperatures.

Two of the authors of this work (D.B. and C.M.) synthesized, by a solution combustion technique based on α-alanine or urea fuels, pure and doped lanthanum cobaltites with relatively high specific

* Corresponding author. Tel.: +40 21 4023883; fax: +40 21 3185900.
*E-mail address:* g_bozga@chim.upb.ro (G. Bozga).

0926-3373/$ – see front matter © 2008 Elsevier B.V. All rights reserved.
doi:10.1016/j.apcatb.2008.06.008

**Nomenclature**

| | |
|---|---|
| $a_v$ | specific gas–solid surface area ($m^2_{GS}/m^3_{bed}$) |
| $C_A$ | molar concentration of methane in the catalyst (kmol/$m^3$) |
| $C_t$ | total molar concentration of the gas phase (kmol/$m^3$) |
| $d_p$ | mean particle diameter (m) |
| $D_A$ | methane molecular diffusion coefficient ($m^2$/s) |
| $E_{ar}$ | apparent activation energy of methane combustion process (J $mol^{-1}$) |
| $K_O$ | adsorption equilibrium constant of oxygen ($atm^{-1}$) |
| $k_1$ | rate constant when reaction involves adsorbed oxygen (kmol $kg^{-1}$ $s^{-1}$ $Pa^{-1}$) |
| $k_2$ | rate constant when reaction involves lattice oxygen (kmol $kg^{-1}$ $s^{-1}$ $atm^{-1}$) |
| $k_G$ | gas to particle mass transfer coefficient of methane (m/s) |
| $k_m$ | apparent reaction rate constant (kmol $kg^{-1}$ $s^{-1}$ $atm^{-1}$) |
| $N_A$ | methane flux transferred to external catalyst surface (kmol $m^{-2}$ $s^{-1}$) |
| $p_A$ | partial pressure of methane (atm) |
| $p_O$ | partial pressure of oxygen (atm) |
| $r$ | combustion rate reported to mass of catalyst (kmol $kg^{-1}$ $s^{-1}$) |
| $r_{A,S}$ | combustion rate reported to catalyst bed volume (kmol $m^{-3}_{bed}$ $s^{-1}$) |
| $R$ | universal gas constant 0.082 $m^3$ atm (kmol$^{-1}$ $K^{-1}$) |
| $Re_p$, $Sc$ | Reynolds and Schmidt numbers |
| $T$ | temperature (K) |
| $u$ | superficial gas velocity in the packed bed (m/s) |
| $y_A$, $y_{A,S}$ | mole fractions of methane in the flowing gas and the external catalyst surface, respectively |

*Greek letters*

| | |
|---|---|
| $\varepsilon$ | bed porosity ($m^3_{gas}/m^3_{bed}$) |
| $\eta$ | gas dynamic viscosity (kg/(m s)) |
| $\Delta\nu$ | variation in number of moles for the oxidation reaction |
| $\nu_A$ | stoichiometric coefficient of methane |
| $\rho$ | gas density (kg/$m^3$) |
| $\rho_{bed}$ | catalyst density in the bed (kg/$m^3$) |

area for this class of compounds [14]. The first objective of this study was to compare the catalytic activities of these pure and doped lanthanum cobaltites in respect with the activity of a commercial $Pt/Al_2O_3$ catalyst currently used for VOC combustion (Engelhard ESCAT 26 with 0.5 wt.% Pt). The reference reaction we considered was the combustion of methane, one of the most resistant compounds to oxidation and therefore often employed in catalytic combustion tests. The results evidenced better combustion activities of the pure and cerium-doped lanthanum cobaltites prepared by using α-alanine fuel, comparing with the Pt (0.5%)/$Al_2O_3$ catalyst. A second objective of this work was to investigate the kinetics of the methane combustion on the tested catalysts. For the lean methane mixtures we tested, the experimental data are reasonably well fitted by a first-order kinetics in respect with methane. Our estimated activation energy values are in good agreement with the data published by other authors for catalysts having similar structures.

## 2. Experimental

### 2.1. Perovskite catalysts synthesis

The catalysts we tested were pure lanthanum cobaltite ($LaCoO_3$), a strontium doped lanthanum cobaltite ($La_{0.8}Sr_{0.2}CoO_3$) and a cerium-doped lanthanum cobaltite ($La_xCe_{1-x}CoO_3$; $x = 0.1$, 0.2), prepared by combustion method using α-alanine or urea fuels. This preparation technique allows good control on the final stoichiometry of catalyst, favouring relatively high porosity and specific surface area. The nature of fuel employed has an important influence on the morphology of the product and consequently on their catalytic properties. The details of the synthesis method are described in a previous work [14]. In a similar way, cerium-doped lanthanum cobaltites are synthesized from $La(NO_3)_3{\cdot}6H_2O$, $(NH_4)_2Ce(NO_3)_6$, $Co(NO_3)_2{\cdot}6H_2O$ (Fluka, 99%) and the corresponding quantity of α-alanine or urea, at a molar ratio $La(NO_3)_3$:$(NH_4)_2Ce(NO_3)_6$:$Co(NO_3)_2$:α-alanine/urea = $1-x$:$x$:1:2/4.2 ($x = 0.1$, 0.2).

### 2.2. Catalysts characterization

Perovskite X-ray diffraction data were collected using a Shimadzu XRD 6000 diffractometer with Cu $K_\alpha$ radiation at a step of 0.02°/s in the range $2\theta = 10$–70°. XRD data of lanthanum cobaltite samples obtained by both α-alanine and urea precursors have proved that all the samples are single phase with distorted rhombohedral perovskite structure (Fig. 1). Besides the perovskite phase, in the cerium-doped oxide XRD patterns $CeO_2$ and $Co_3O_4$ cubic phases are present that were identified as catalytically active species [4].

The synthesis method of tested catalysts, their crystallite size, $D_{012}$ (calculated with Scherrer's equation from full width at half-maximum of the X-ray reflection from $2\theta \approx 23°$) and the specific surface area values measured on Quantachrom Autosorb 1C (after the degassing of samples at 300 °C, 4 h) are listed in Table 1. All further references to these catalysts will be based on the abbreviations introduced in this table. As observed from Table 1, the specific surface area values of the samples prepared by using alanine as fuel are higher than those obtained by using urea. Also, in the case of the catalysts obtained by alanine route, the

**Table 1**
Synthesis conditions, crystallite size and specific surface area for the tested catalysts

| Abbreviation | Compound | Type of precursor | Calcination conditions | $D_{012}$ (nm) | $S$ ($m^2$/g) |
|---|---|---|---|---|---|
| R | $Pt/Al_2O_3$ | | | | 97.02 |
| LCA | $LaCoO_3$ | α-Alanine | 600 °C, 3 h | 19 | 39.57 |
| LSCA | $La_{0.8}Sr_{0.2}CoO_3$ | α-Alanine | 1000 °C, 4 h | 23 | 45.01 |
| LCCA | $La_{0.9}Ce_{0.1}CoO_3$ | α-Alanine | 600 °C, 3 h | 17 | 42.34 |
| LCU | $LaCoO_3$ | Urea | 700 °C, 5 h | 20 | 25.05 |
| LCCU1 | $La_{0.9}Ce_{0.1}CoO_3$ | Urea | 1000 °C, 4 h | 42 | 21.43 |
| LCCU2 | $La_{0.8}Ce_{0.2}CoO_3$ | Urea | 1000 °C, 4 h | 22 | 20.95 |

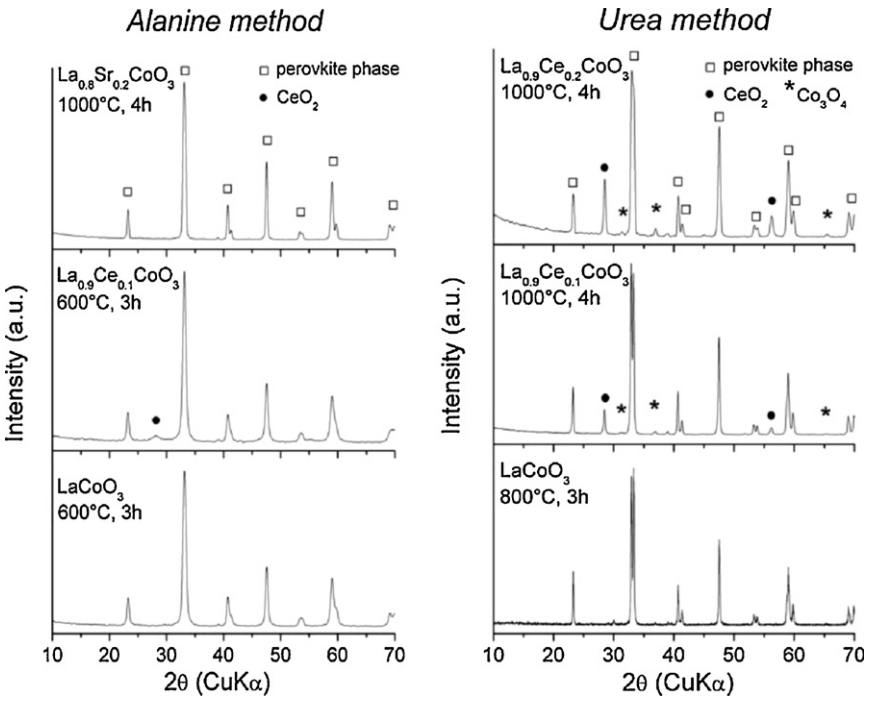


**Fig. 1.** XRD patterns of pure and doped lanthanum cobaltite.

lanthanum substitution either by $Sr^{2+}$ or by $Ce^{4+}$, led to higher values of the specific surface area. Oppositely, in the case of the perovskites obtained by urea method, the lanthanum substitution with $Ce^{4+}$ caused a decrease of specific surface area. The specific surface area values of the perovskites obtained by alanine method are higher than the values reported in literature for materials having similar structure [4,5,12].

### 2.3. Experimental set-up and catalytic tests

The experimental installation used in the catalytic combustion study is depicted in Fig. 2. A quantity of catalyst powder (0.1–0.2 g) was loaded in a quartz tube reactor (i.d. = 4 mm) between two layers of quartz beads to assure uniform gas flow in the catalyst bed. The quartz tube was placed in a furnace provided with temperature controller. The reaction temperature was monitored at the centre of the catalyst bed with a Pt/Rh thermocouple having the accuracy of 0.1 °C (placed in a 1 mm external diameter thermowell). The methane combustion was performed with oxygen from air, provided by a compressor. The gaseous mixture of methane and air was fed into reactor at flow rates varying in the range of 1500–12,000 $cm^3\ h^{-1}$ and various methane concentrations (1.2 and 2.2 mol%). The air and methane flow rates were measured and regulated by electronic controllers. The product

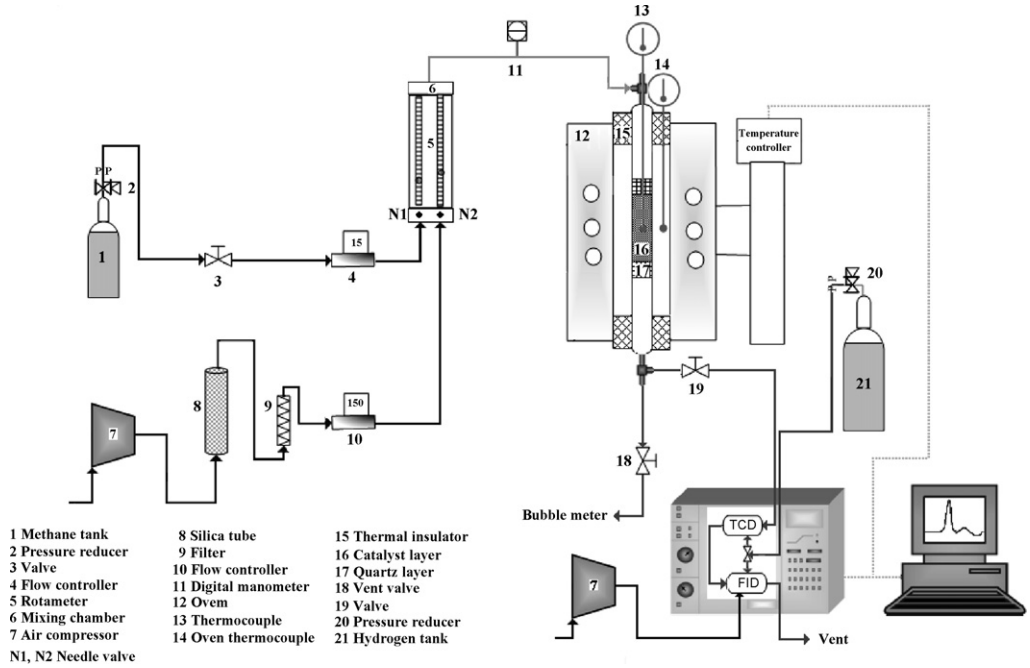


**Fig. 2.** Schematic diagram of the experimental set-up for methane catalytic combustion.

mixture composition was measured on-line by gas chromatography, using a Varian™ CP-3800 GC equipped with methanizer, FID and TCD detectors, a molecular sieve 5 Å column for $N_2$, $O_2$, CO, $CH_4$ and a Hayesep Q column, respectively, for $CO_2$ analysis. The calibration of the chromatograph was performed by using an etalon gaseous mixture provided by Messer™.

The pressure drop in the reactor was always lower than 0.2 bar, thus it was considered that experiments were conducted at atmospheric pressure. Before the combustion tests, each perovskite catalyst was activated in air (6000 $cm^3\ h^{-1}$) for 2 h at 600 °C, to remove adsorbed species [15]. $Pt/Al_2O_3$ catalyst was activated and stabilized for 2 h at 600 °C under reaction conditions [16]. The methane conversion was calculated from the concentration measurements of methane and carbon oxides at the inlet and the outlet of the reactor. To check the reproducibility of the results, the methane conversion curve was measured twice for each catalyst, by traversing the temperature interval in both upward and downward directions. The consistency of the experimental data was checked by calculating the carbon balance around the reactor, from the measurements of inlet and outlet flow rates and concentrations of carbon compounds, respectively. The carbon balance closed with errors smaller than 5% for all the experiments.

In the case of the Pt/alumina catalyst, particle size practically free of internal diffusion effects was identified by experiments on different dimension classes, obtained by crushing the commercial pellets and sieving. The combustion experiments were carried out in identical working conditions, on the higher temperature and flow rate domains. The results show that the influence of the internal diffusion can be practically neglected, for particle dimensions smaller than 250 μm. All the reported experiments were further carried out with this class of catalyst particles. The pore size distribution for the Pt/alumina catalyst, measured on an Autosorb-1 Quantachrome apparatus, showed a range of pores size from 50 to 250 Å, with a mean pore diameter of 236 Å (BJH method).

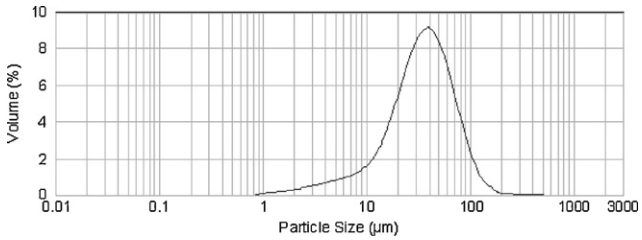


**Fig. 3.** Particle size distribution for LCCA perovskite catalyst.

The experiments on perovskite oxide catalysts were carried out with the materials under the form of powder, as resulted from the synthesis method (particles diameter between 50 and 150 μm). For the most active catalyst in this class (LCCA), the analysis of pore size distribution showed a range of dimensions from 100 to 2000 Å, with an average pore diameter of 1240 Å (Autosorb-1 Quantachrome apparatus, BJH method). An average grain size of 35.1 μm was determined for this perovskite from the grain size distribution, measured on a Mastersizer Hydro 2000S instrument (Fig. 3). SEM images presenting the morphology of some lanthanum cobaltite compounds we tested are also given in Fig. 4.

## 3. Results and discussion

In almost all the experiments, water and carbon dioxide were the only products; however, scarce quantities of carbon monoxide were detected for LCCU1 catalysts at temperatures above 700 °C, where homogeneous combustion contribution becomes significant.

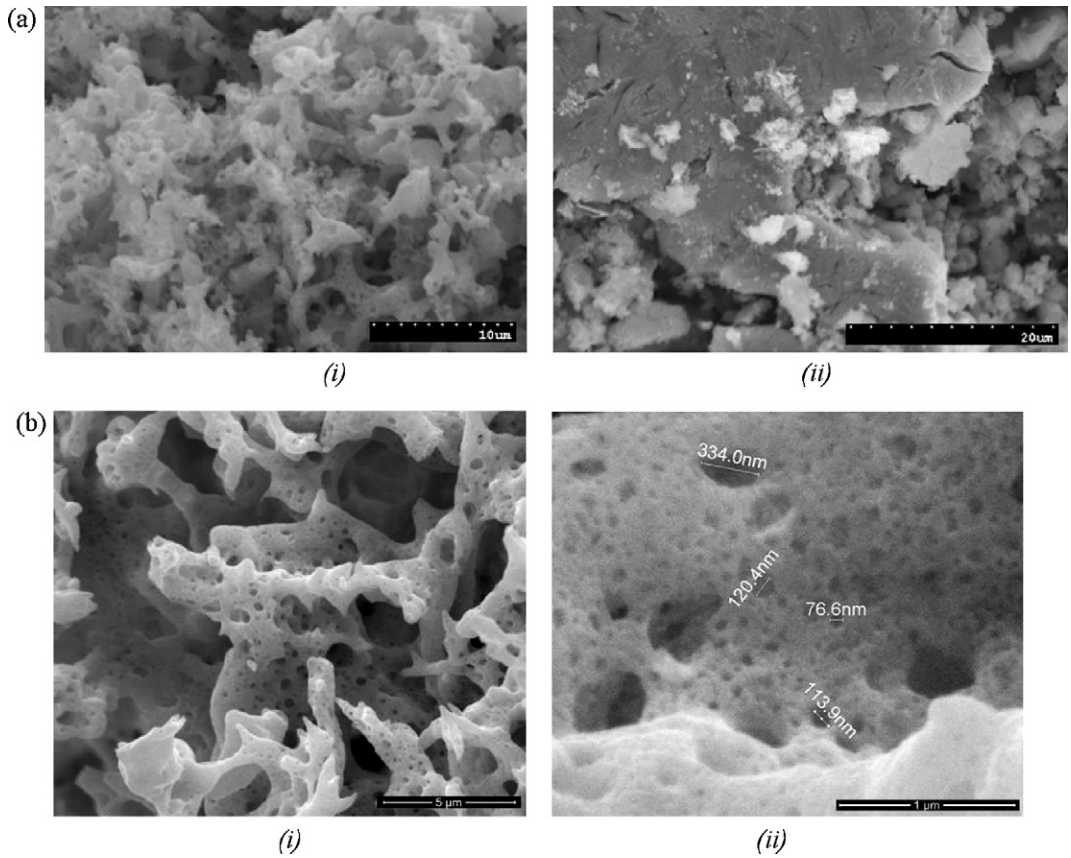


**Fig. 4.** SEM images of the lanthanum cobaltite catalysts. (a) LCA: 3500× (i) and LCU: 2500× (ii); (b) LCCA: 15,000× (i) and 100,000× (ii).

**Table 2**
Activities of tested catalysts (1.2% $CH_4$; GHSV = 15,000 $cm^3\,h^{-1}\,g^{-1}$)

| Catalyst | $T_{10}$ (°C) | $T_{50}$ (°C) | $T_{99}$ (°C) |
|---|---|---|---|
| R | 455 | 550 | 628 |
| LCA | 397 | 480 | 619 |
| LSCA | 456 | 562 | 745 |
| LCCA | **342** | **427** | **547** |
| LCU | 405 | 507 | 679 |
| LCCU1 | – | 655 | 874 |
| LCCU2 | – | 636 | 866 |
| Thermal combustion (TC) | 804 | 822 | 873 |

Catalytic activity in methane combustion, of perovskite-type oxides mentioned above, was assessed by measuring the level of methane conversion obtained in identical working conditions.

The values of reaction temperature corresponding to 10%, 50% and 99% methane conversions ($T_{10}$, $T_{50}$ and $T_{99}$) for the tested catalysts are given in Table 2 and the conversion–temperature curves (light-off curves) for the most active ones are presented in Fig. 5. Some of these catalysts proved significant higher activities as compared with published results on similar materials leading to total conversions of methane within the temperature interval of 550–680 °C [4,5,15]. As observed from Table 2 and Fig. 5, the catalytic activities of pure and cerium-doped lanthanum cobaltites prepared by using α-alanine fuel (LCA and LCCA) and the pure lanthanum cobaltite prepared by urea fuel (LCU) are higher than that of the commercial $Pt/Al_2O_3$ (0.5% Pt). However, it is to notice that LCU catalyst is more active than the reference commercial one, only at temperatures below 620 °C. The difference between the activities of the pure lanthanum cobaltites prepared by alanine (LCA) and urea (LCU) methods is explained by their morphology. SEM images revealed that LCA catalyst presents a higher porosity with micropores and voids having the aperture around 50 nm and lower degree of agglomerates formation comparing with LCU one (Fig. 4a). Among all the catalysts tested, the highest activity for methane combustion was observed at LCCA perovskite (as evidenced by bold numbers in Table 2). When compared with the results reported by other authors for similar catalysts, the $T_{50}$ value of LCCA catalyst is lower with approximately 50 °C for close working conditions [4,5]. The superior activity of this catalyst can be explained by its relatively higher specific surface area and the presence of $CeO_2$ and cubic $Co_3O_4$ catalytically active species in its structure [4]. SEM analysis of LCCA catalyst showed a spongy but continuous morphology and the existence of a large amount of both micropores and nanopores (Fig. 4b).

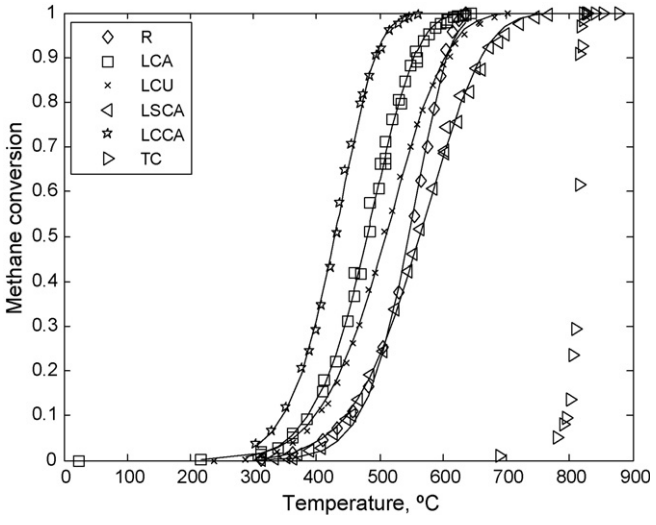


**Fig. 5.** Light-off curves for methane combustion on different catalysts. The points represent measured and the lines calculated values (according to the first-order power law model); feed methane concentration 1.2 mol%; space velocity, 15,000 $cm^3\,h^{-1}\,g^{-1}$.

The results presented in Table 2 and Fig. 5 are evidencing also that, unlike the case of alanine route perovskites, the substitution of lanthanum ions with cerium in the perovskites prepared by urea method have not led to a significant increase of catalytic activity.

All the light-off curves used in the comparisons of catalytic activities were obtained on fresh catalysts. Nevertheless, during our experimental investigations a certain extent of deactivation was observed on both LCCA and Pt/alumina catalysts. As a first evaluation of these phenomena, we measured the decrease of specific surface area for the LCCA catalyst after approximately 50 h on-stream time at a temperature of 450 °C. This evidenced a diminution of specific surface area from 39.57 to 21.5 $m^2/g$. However, we have not observed a methane conversion decrease of the same magnitude as the decline of surface area (the measured conversion decrease due to deactivation was around 10%). Similarly, from measurements of methane conversion at 605 °C during 50 h of on-stream time on the reference Pt/alumina catalyst, we observed an initial decrease of activity followed by a trend of stabilization at a level of approximately 60% relatively to initial one. Consequently, in order to evaluate the commercial value of the LCCA catalyst further studies are necessary concerning its resistance to deactivation in the expected working conditions (nature of the VOC, temperature, etc.).

### 3.1. Combustion process kinetics

#### 3.1.1. Methane combustion kinetics on the tested perovskite catalysts

The mechanism of the methane oxidation on the surface of a perovskite catalyst was explained by the participation to the surface reaction of two oxygen species, the adsorbed oxygen and the bulk lattice oxygen, respectively [17–19]. The involvement of one or the other oxygen species predominates, depending on the reaction temperature. The adsorbed oxygen is more active and reacts with methane at lower temperature than lattice oxygen. In a first possible mechanism, predominating at lower temperatures, the reaction occurs between non-dissociated adsorbed oxygen and gaseous methane (Eley-Rideal mechanism), whereas in a second one, predominating at higher temperatures, the surface process is following a Mars-van Krevelen scheme that involves atomic oxygen originated from catalyst lattice.

An expression of the reaction rate based on the Eley-Rideal mechanism was proposed in several published works, assuming that the rate determining step on the catalyst surface is the chemical reaction of non-dissociated oxygen adsorbed molecules and non-adsorbed methane molecules [19]:

$$r = k_1\, p_A \frac{K_O\, p_O}{1 + K_O\, p_O} \quad (1)$$

Augmenting the temperature, the concentration of adsorbed oxygen on the catalyst surface decreases and simultaneously the lattice oxygen becomes more reactive, so that, on the highest temperature domain, the surface combustion process is occurring mainly with the participation of lattice oxygen. If the combustion process takes place in oxygen excess at high temperatures, the incorporation of gaseous oxygen in oxide lattice is fast, thus the reaction rate is zero-order with respect to the oxygen partial pressure:

$$r = k_2\, p_A \quad (2)$$

By including the two mechanisms contributions, the overall methane combustion rate has the expression:

$$r = k_1 p_A \frac{K_O p_O}{1 + K_O p_O} + k_2 p_A \quad (3)$$

As our experiments were carried out in high oxygen excess, the oxygen concentration is practically constant along the catalyst bed and the rate equation (3) can be simplified to a pseudo-first-order expression with respect to methane:

$$r = k_m p_A; \qquad k_m = k_1 \frac{K_O p_O}{1 + K_O p_O} + k_2 \quad (4)$$

where $k_m$ is practically dependent only on reaction temperature. This temperature dependence is expressed by the Arrhenius equation, $k_m = k_{m0} \exp(-E_{ar}/RT)$, including an apparent activation energy, $E_{ar}$.

In order to evaluate the parameters $k_{m0}$ and $E_{ar}$ appearing in the first-order rate expression (4), we used a pseudo-homogeneous plug-flow model of the experimental reactor [20]. The contribution of axial mixing to the mass transport inside the catalyst bed was neglected, considering that the ratio of catalyst bed height to particle diameter is relatively high ($L/d_p > 150$) for all the experiments.

The estimated values of parameters $k_{m0}$ and $E_{ar}$ for the tested catalysts are presented in Table 3. The corresponding calculated conversions for the most active catalysts are presented, comparatively with the measured ones, in Fig. 5. As seen, a good adequacy of the first-order kinetic model to experimental data has been obtained. It is also worth to mention the good concordance of the calculated values of apparent activation energy with the values reported by other authors for the same process, on catalysts having similar structures (Table 3). The magnitude order of calculated activation energies for the combustion process (all higher than $6.5 \times 10^4$ J/mol) are specific for kinetic regimes free of mass transport influences.

The influence of the gas flow rate on the methane conversion for the most active catalyst (LCCA) is presented in Fig. 6. As expected, the temperature necessary for complete combustion is increasing with the gas flow rate, due to the decrease of the contact time between reactants and catalyst.

To check the influence of the gas–solid mass transfer step on process kinetics, we evaluated the external dimensionless concentration gradient of methane on the highest temperature working domain, for the most active catalyst.

The methane mass flux transferred toward the external catalyst surface, including diffusion and convection contributions, can be calculated by the expression [20,21]:

$$N_A = \frac{k_G C_t}{f_A}(y_A - y_{A,S}); \qquad f_A = 1 + \delta_A \bar{y}_A; \qquad \bar{y}_A = \frac{y_{A,S} + y_A}{2}; \qquad \delta_A = \frac{\Delta\nu}{\nu_A} \quad (5)$$

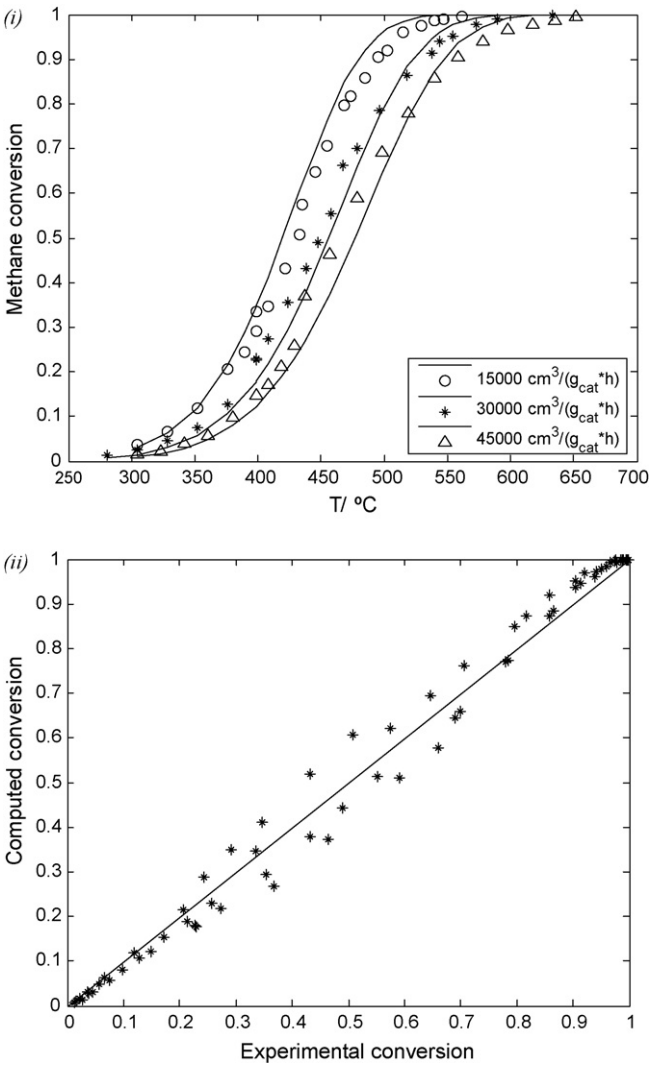


**Fig. 6.** Conversion–temperature curves for different feed flow rates (feed methane concentration 1.2 mol%); the points represent measured and the lines calculated values (according to the first-order power law model); (i) conversion vs. temperature diagram; (ii) parity diagram.

As the predominant reaction is methane combustion to $CO_2$ (where $\Delta\nu = 0$) and the methane concentration is very low ($\bar{y}_A < 0.02$), the value considered in calculus was $f_A = 1$.

The methane balance on the volume unit of catalyst bed is expressed by the equation:

$$a_v k_G C_t (y_A - y_{A,S}) = r_{A,S}; \qquad r_{A,S} = k_m p y_{A,S} \rho_{bed} \quad (6)$$

**Table 3**
Kinetic parameters in the first-order rate expression (4)

| Catalyst | $k_{r0}$ (kmol kg$^{-1}$ s$^{-1}$ atm$^{-1}$) this work | $E_{ar}$ (J mol$^{-1}$) this work | $E_{ar}$ (J mol$^{-1}$) literature values [14] |
|---|---|---|---|
| LCA | $6.643 \times 10^1$ | $8.36 \times 10^4$ | $9.25 \times 10^4$ |
| LSCA | $0.990 \times 10^1$ | $7.97 \times 10^4$ | – |
| LCCA | $8.054 \times 10^1$ | $8.29 \times 10^4$ | $8.3 \times 10^4$ |
| LCU | $0.937 \times 10^1$ | $7.41 \times 10^4$ | $9.25 \times 10^4$ |
| LCCU1 | $5.345 \times 10^{-1}$ | $6.58 \times 10^4$ | $8.3 \times 10^4$ |
| LCCU2 | $0.136 \times 10^1$ | $7.16 \times 10^4$ | $9.7 \times 10^4$[a] |
| Thermal combustion (TC) | – | $2.30 \times 10^5$ | $2.57 \times 10^5$ |

[a] Value from Ref. [3].

The gas–solid mass transfer coefficient was evaluated from the equation proposed by Yoshida et al. [22]:

$$j_D = \frac{k_G}{u} Sc^{2/3} = 0.84 Re_p^{-0.51}; \qquad Re_p = \frac{u\rho}{0.9 a_v \eta}; \qquad a_v = \frac{6(1-\varepsilon)}{d_p}; \qquad Sc = \frac{\eta}{\rho D_A} \tag{7}$$

Assuming ideal behaviour of the reaction mixture and a first-order reaction kinetics in respect with methane, one obtains the following global combustion rate expression:

$$r_{A,S} = K \rho_{bed} C_A; \qquad C_A = C_t y_A; \qquad \frac{1}{K} = \frac{1}{k_m RT} + \frac{\rho_{bed}}{k_G a_v} \tag{8}$$

In this expression, $1/K$ represents the overall resistance opposed to the combustion process by the surface steps (first term) and external mass transfer, respectively (second term). The external dimensionless concentration gradient of methane or, equivalently, the weight of the resistance opposed by external mass transfer, is given by the expression:

$$\frac{y_A - y_{A,S}}{y_A} = \frac{K \rho_{bed}}{k_G a_v} \tag{9}$$

The values of this ratio calculated along the catalyst bed for the most active catalyst we tested, are smaller than 0.01 on the entire working domain. Consequently, the influence of the gas–solid mass transfer on the overall process kinetics can be neglected for all the tested catalysts.

*3.1.2. Methane combustion kinetics on Pt/alumina catalyst*

To describe the surface reaction rate of methane combustion, several kinetic models derived by Langmuir Hinshelwood or Eley-Rideal theories were proposed, considering that the reaction takes place between adsorbed oxygen and adsorbed or gas phase methane molecules [23–25]. When working in high excess of oxygen, as is the case of present work, the variation of oxygen concentration during the combustion process can be neglected, so that these rate expressions can be simplified to first-order forms in respect with methane concentration. Therefore, simple power law empirical kinetic models of different orders were also used by different authors for combustion kinetics, especially at low methane concentrations.

We tested on our data all these kinetic expressions, with their original parameter values, but no one fitted satisfactorily the experimental light-off curves. This could be explained by differences in physical characteristics of the catalyst (gas–solid contact surface area, noble metal distribution on the surface of alumina, etc.). By re-fitting these kinetic models on our experimental data, the most appropriate proved to be the first-order model presented in Table 4. The value of apparent activation energy (140,320 J/mol), calculated by this kinetic model, is close to other published results (131,020 J/mol [26]; 150,690 J/mol [27]; 146,930 J/mol [28]; 134,790 J/mol [29]).

As the catalyst grains size and working conditions for the Pt/alumina experiments were in the same range as for experiments on the LCCA catalyst described above, the influence of the gas–solid mass transfer step on the overall process kinetics is even lower and consequently can be neglected.

**Table 4**
The kinetic model for methane combustion on Pt/alumina catalyst

| |
|---|
| $r_A = k_m p_A$; $k_m = k_0 \exp(-E_a/RT)$ |
| $k_0 = 9.153 \times 10^4$ kmol kg$^{-1}$ s$^{-1}$ atm$^{-1}$; $E_a$ = 140,320 J/mol |

## 4. Conclusions

The paper presents an investigation of the combustion catalytic activity of some perovskite oxides prepared by solution combustion technique, comparatively with a commercial 0.5 wt.% $Pt/Al_2O_3$ catalyst.

The pure lanthanum cobaltite catalysts obtained by alanine (LCA) or urea (LCU) as fuel show superior or similar catalytic activity with the commercial one. The highest activity was observed for $La_{0.9}Ce_{0.1}CoO_3$ (LCCA) obtained by this method at 600 °C. The superior catalytic activity of the perovskite oxides obtained by alanine route is due to the higher specific surface area values and their more adequate morphology.

To describe the methane combustion kinetics, we adopted a simplified first-order power law expression in respect with methane, which fits well the experimental data, due to the high oxygen excess in the reaction mixture. The estimated values of activation energy are in good agreement with published data for methane combustion on catalysts having similar structures.

As a conclusion, the cerium-doped lanthanum cobaltite perovskite synthesized by alanine method can be considered a good candidate to replace the noble metal catalysts for VOC combustion processes. Nevertheless, further studies are necessary regarding the conditioning and resistance to deactivation phenomena specific for commercial exploitation.

## Acknowledgements

The authors acknowledge the financial support of the Romanian National Authority for Scientific Research in the development of this work (CEEX no. 14/2006). Also, the authors gratefully thank to Catalytic Reaction Engineering for Energy and Environment-CRE$^3$ Group, Politecnico di Torino, Italy, for some of the SEM images presented in this work and to Dr. F. Papa for specific surface area measurements.

## References

[1] E. Campagnoli, A. Tavares, L. Fabbrini, I. Rossetti, Y.A. Dubitsky, A. Zaopo, L. Forni, Appl. Catal. B 55 (2005) 133–139.
[2] M. Alifanti, M. Florea, V.I. Parvulescu, Appl. Catal. B 70 (2007) 400–405.
[3] L. Huang, M. Bassir, S. Kaliaguine, Mater. Chem. Phys. 101 (2007) 259–263.
[4] J. Kirchnerova, M. Alifanti, B. Delmon, Appl. Catal. A 231 (2002) 65–80.
[5] R. Leanza, L. Rossetti, L. Fabbrini, C. Oliva, L. Forni, Appl. Catal. B 28 (2000) 55–64.
[6] H. Huang, Y. Liu, W. Tang, Y. Chen, Catal. Commun. 9 (2008) 55–59.
[7] S. Specchia, A. Civera, G. Saracco, Chem. Eng. Sci. 59 (2004) 5091–5098.
[8] A. Civera, G. Negro, S. Specchia, G. Saracco, V. Specchia, Catal. Today 100 (2005) 275–281.
[9] S. Specchia, A. Civera, G. Saracco, V. Specchia, Catal. Today 117 (2007) 427–432.
[10] G.L. Chiarello, J.-D. Grunwaldt, D. Ferri, F. Krumeich, C. Oliva, L. Forni, A. Baiker, J. Catal. 252 (2007) 127–136.
[11] J.M. Giraudon, A. Elhachimi, F. Wyrwalski, S. Siffert, A. Aboukais, J.F. Lamonier, G. Leclercq, Appl. Catal. B 75 (2007) 157–166.
[12] B. Bialobok, J. Trawczynski, W. Mista, M. Zawadzki, Appl. Catal. B 72 (2007) 395–403.
[13] S. Royer, H. Alamdari, D. Duprez, S. Kaliaguine, Appl. Catal. B 58 (2005) 273–288.
[14] D. Berger, C. Matei, F. Papa, G. Voicu, V. Fruth, Prog. Solid State Chem. 35 (2007) 183–191.
[15] M. Alifanti, N. Blangenois, M. Florea, B. Delmon, Appl. Catal. A 280 (2005) 255–265.
[16] L. Van de Beld, Air purification by catalytic oxidation in an adiabatic packed bed reactor with periodic flow reversal, PhD Thesis, Netherlands, 1995, 14 pp.
[17] H. Arai, T. Yamada, K. Eguchi, T. Seiyama, Appl. Catal. 26 (1986) 265–276.
[18] S. Kaliaguine, A. Van Neste, V. Szabo, J.E. Gallot, M. Bassir, R. Muzychuk, Appl. Catal. A 209 (2001) 345–358.
[19] V. Szabo, M. Bassir, J.E. Gallot, A. Van Neste, S. Kaliaguine, Appl. Catal. B 42 (2003) 265–277.
[20] G.F. Froment, K. Bischoff, Chemical Reactor Analysis and Design, John Wiley, N.Y, 1979, pp. 143–150.
[21] R.B. Bird, E.S. Stewart, E.N. Lightfoot, Transport Phenomena, John Wiley, NY, 1960, pp. 636–642.
[22] F. Yoshida, D. Ramaswami, O.A. Hougen, AIChE J. 8 (1962) 5–11.

[23] G.I. Golodets, *Heterogeneous Catalytic Reactions Involving Molecular Oxygen*, Stud. Surf. Sci. Catal., vol. 15, Elsevier, Amsterdam, 1983, pp. 126–149.
[24] L. Ma, D.L. Trimm, C. Jiang, Appl. Catal. A 138 (1996) 275–283.
[25] S.T. Seyama, Catal. Rev.-Sci. Eng. 34 (1992) 281–300.
[26] S.T. Kolaczkowski, S. Serbetcioglu, Appl. Catal. A 138 (1996) 199–214.
[27] W.J. Kuper, M. Blaauw, F. van der Berg, G.H. Graaf, Catal. Today 47 (1999) 377–389.
[28] K. Otto, Langmuir 5 (1989) 1364–1369.
[29] X. Song, W.R. Wiliams, L.D. Schmidt, R. Aris, Combust. Flame 84 (1991) 292–311.